



The 13 million year Cenozoic pulse of the Earth

Jiasheng Chen^{a,b,c}, Vadim A. Kravchinsky^{b,*}, Xiuming Liu^{a,c}



^a School of Geographical Sciences, Fujian Normal University, Fuzhou 350007, China

^b Department of Physics, University of Alberta, Edmonton, Alberta T6G 2E1, Canada

^c Key Laboratory of Western China's Environmental Systems, Research School of Arid Environment & Climate Change, Lanzhou University, Lanzhou 730000, China

ARTICLE INFO

Article history:

Received 12 January 2015

Received in revised form 18 September 2015

Accepted 21 September 2015

Available online 13 October 2015

Editor: M. Frank

Keywords:

Cenozoic

Cenozoic climate change

geomagnetic reversals

oxygen isotope

tectonic plate subduction

ABSTRACT

The geomagnetic polarity reversal rate changes radically from very low to extremely high. Such process indicates fundamental changes in the Earth's core reorganization and core–mantle boundary heat flow fluctuations. However, we still do not know how critical such changes are to surface geology and climate processes. Our analysis of the geomagnetic reversal frequency, oxygen isotope record, and tectonic plate subduction rate, which are indicators of the changes in the heat flux at the core mantle boundary, climate and plate tectonic activity, shows that all these changes indicate similar rhythms on million years' timescale in the Cenozoic Era occurring with the common fundamental periodicity of ~13 Myr during most of the time. The periodicity is disrupted only during the last 20 Myr. Such periodic behavior suggests that large scale climate and tectonic changes at the Earth's surface are closely connected with the million year timescale cyclical reorganization of the Earth's interior.

© 2015 Elsevier B.V. All rights reserved.

1. Introduction

Earth's magnetic field has flipped from a normal to a reverse polarity many times in the Cenozoic Era. The polarity is recorded during sea floor formation in the spreading zones when magma cools and becomes magnetized by the geomagnetic field. Magnetic stripes with alternating normal and reverse polarities are produced parallel to the ridge axis (Vine and Matthews, 1963). Based on the assumption that spreading rates in the South Atlantic were smoothly varying, Cande and Kent (1995) calibrated ages of the magnetic stripes and established the CK95 geomagnetic polarity time scale (GPTS). Studies suggest that the geomagnetic polarity reversal rate is an indicator of the Earth's core–mantle boundary (CMB) heat flow fluctuations that exert an impact on global scale climate change by mantle plume related volcanism (Courillot and Olson, 2007; Sobolev et al., 2011; Biggin et al., 2012; Rampino and Prokoph, 2013). These phenomena suggest a virtual connection between deep Earth behavior and long-term climate change on a million year scale; however, it is not known how these processes are associated in the Cenozoic Era.

Previous studies have suggested that geomagnetic reversal frequency show primary 15 Myr cycles over the last 100 Ma (Mazaud et al., 1983; Mazaud and Laj, 1991) and ~33 Myr cycles over the last 300 Ma (Rampino and Stothers, 1984; Pal and Creer, 1986). As

for climate change, there has been no identification of any significant long-term periodicities in the Cenozoic marine $\delta^{18}\text{O}$ data from earlier research (Rampino and Stothers, 1987). The climate changes over the Cenozoic Era have now been well reconstructed using $\delta^{18}\text{O}$ (Zachos et al., 2001). Cenozoic marine $\delta^{13}\text{C}$ data, which are an indicator of carbon cycle changes, show that the 9 Myr cyclicity (Boullila et al., 2012) could possibly be linked to the long-term orbital eccentricity modulation. Our study aims to explore if there is any common global rhythm imprinted in the geomagnetic and the climatic records that can be indicative of the existence of such virtual connection.

2. Methods and results

To compare geomagnetic reversal frequency and climate variation cyclicity in the Cenozoic Era, we calculated the reversal frequency with a moving window for the last 73 Ma using the GPTS revised by Gee and Kent in 2007 (Gee and Kent, 2007). The window width is 2 Myrs and the time step interval is 0.1 Myr. The red line in Fig. 1a is the variation in reversal frequency over the last 73 Ma. The minimum and maximum reversal frequency values between 73 and 30 Ma are 0.5 Myr^{-1} and 3.5 Myr^{-1} , respectively. From 30 Ma to the present day, the minimum values increase almost linearly from 0.5 Myr^{-1} at 31.8 Ma to 3 Myr^{-1} at 6 Ma, the maximum values increase from 4 Myr^{-1} at 29.3 Ma to 6.5 Myr^{-1} at 23 Ma, and further rise to 9.5 Myr^{-1} at 12 Ma. The net difference between the minimum values for both intervals is

* Corresponding author. Tel.: +1 780 4925591.

E-mail address: vadim@ualberta.ca (V.A. Kravchinsky).

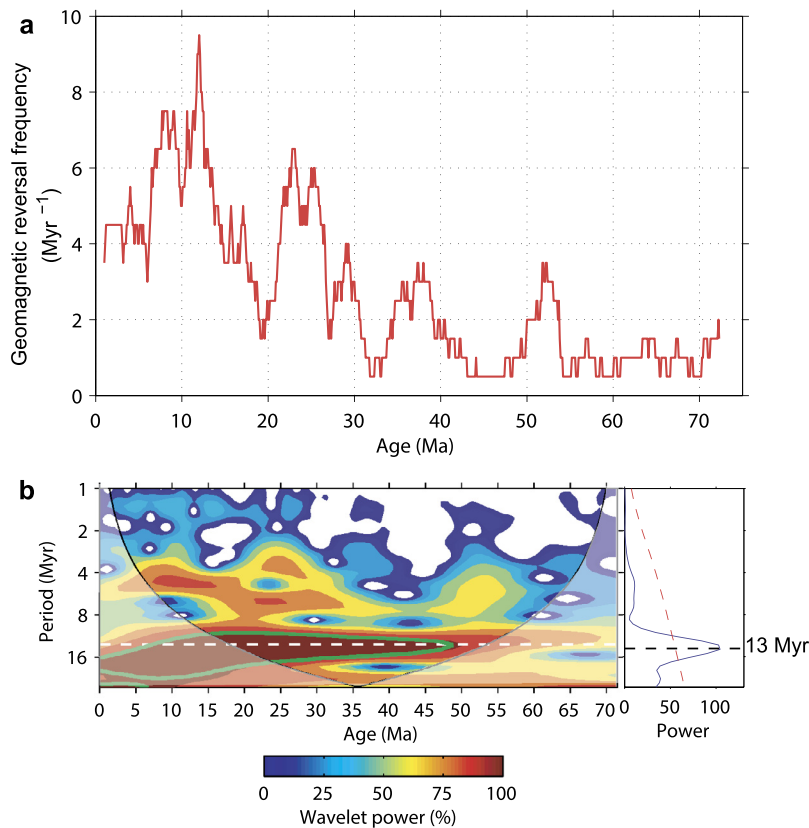


Fig. 1. Variations of geomagnetic polarity reversal frequency. (a) Geomagnetic reversal frequency (red line). (b) Wavelet analysis for reversal frequency. Black solid line corresponds to cone of influence, shadowed area is outside of the cone. Horizontal white dot line in wavelet power spectrum (left) denotes 13 Myr periodicity and green line is 95% significance contour. Black and red dashed lines in global wavelet spectrum (right) denote 13 Myr periodicity and 95% confidence level. (For interpretation of the references to color in this figure legend, the reader is referred to the web version of this article.)

$\sim 3.5 \text{ Myr}^{-1}$. The reversal frequency shows peaks at 52 Ma, 39 Ma, 26–23 Ma and 12 Ma. The difference between these peaks, i.e. periodicity of the high reversal frequency intervals is $\sim 13 \text{ Myr}$.

To evaluate subtle changes through time we performed wavelet analyses on the reversal frequency curve using the method of Torrence and Compo (1998) (Fig. 1b). The Matlab code is from <http://paos.colorado.edu/research/wavelets/>. Mother wavelet is Morlet, the sampling interval is 0.1 Myr, and the lag-1 autocorrelation for the red noise background is 0.72. The wavelet power spectrum demonstrates the prevailing periodicity of 13 Myr between 50 and 10 Ma with a confidence level of 95% (Fig. 1b). A 15 Myr periodicity registered in the geomagnetic polarity record was already proposed in 80s and 90s (Mazaud et al., 1983; Mazaud and Laj, 1991; Marzocchi and Mulargia, 1992). However, the previous result is based on outdated reversal record, our analysis suggests that very similar 13 Myr cycle dominates the geomagnetic reversal frequency record for the last 73 Myr. The periodicity seems to be disrupted during last 10 Myrs, but this interval cannot provide exact estimation as it is outside of the confidence cone.

Furthermore, we searched for any very large scale rhythms registered in the climate global record because a few substantial climate changes have occurred in the Cenozoic Era. Climate changes over the last 67 Myr have been reconstructed by the $\delta^{18}\text{O}$ isotope record of oceanic foraminifera shells (Zachos et al., 2001). The $\delta^{18}\text{O}$ record is sensitive to deep-sea temperature and ice volume changes; a high $\delta^{18}\text{O}$ value corresponds to low temperature and high ice volume. Fig. 2a illustrates the variations of $\delta^{18}\text{O}$ between 67 Ma and the present (Zachos et al., 2001). The $\delta^{18}\text{O}$ record (shown as a blue line) is characterized by a continuously rising long-term trend since 50 Ma (shown as a magenta line) with two large scale temporary decreases. The Cenozoic cooling trend has

been attributed to the drawdown of atmospheric CO_2 due to the increasing continental weathering as a result of the Tibetan Plateau uplift (Garzzone, 2008), or attributed to the slow CO_2 input related to the slow spreading rate as the BLAG hypothesis suggested (Berner et al., 1983). Here we explore the rhythms of the Cenozoic climate change. The long-term trend of $\delta^{18}\text{O}$ is constructed by smoothing the dataset. The trend is nonlinear, therefore we use the nonlinear locally weighted polynomial regression (LOWESS method) where the smoothing parameter is 0.5 which means 50% of the data are used in each fit. Further, we subtract the trend from the original $\delta^{18}\text{O}$ record to evaluate the second order features and their possible cyclicity (green line in Fig. 2a).

Fig. 2b is the output of the wavelet analysis for the detrended $\delta^{18}\text{O}$ record. The wavelet power spectrum shows a primary 13 Myr periodicity between 67 and 17 Ma, and an 8–10 Myr periodicity for 23–0 Ma interval, which is similar to the 9 Myr cycle in the marine $\delta^{13}\text{C}$ record (Boulila et al., 2012). The 13 Myr cycle between 67 and 17 Ma are 65–52, 52–39, 39–26 Ma (red dashed line in Fig. 2a). The periodicity is shorter for the last $\sim 20 \text{ Ma}$, but three peaks can still be accounted. However, the most recent and oldest time intervals are outside the 95% confidence level cone.

It has been suggested that the geomagnetic reversal rate could be closely associated with sea-floor creation and subduction rate (Gaffin, 1987). To explore any million year scale periodicity we used known rates of tectonic plate subduction (Rowley, 2002) shown in Fig. 3a since the data is compiled for the entirety of the world and can represent global tectonic processes. The wavelet power spectrum of the subduction rate (Fig. 3b) also shows a primary $\sim 13 \text{ Myr}$ cycle between 70 and 17 Ma, which coincides with the cyclicity of the geomagnetic reversal rate and $\delta^{18}\text{O}$ records. The subduction rate is somewhat better reconstructed than the

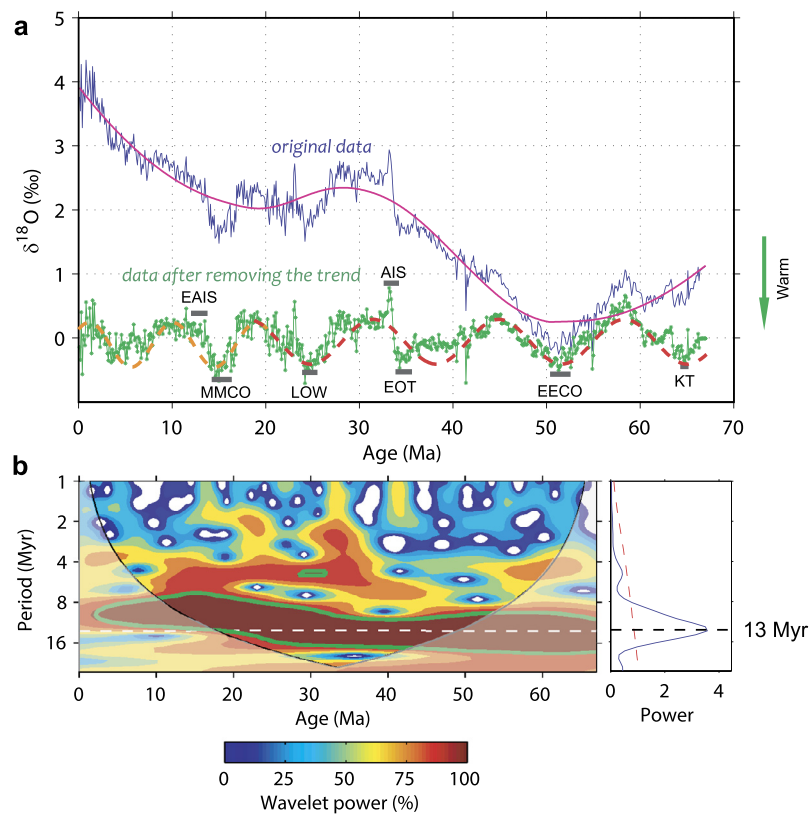


Fig. 2. Variations of $\delta^{18}\text{O}$. (a) Original data (blue line), trend of $\delta^{18}\text{O}$ (magenta line), and detrended $\delta^{18}\text{O}$ (green line). Major transitions in $\delta^{18}\text{O}$ record: MMCO – mid Miocene climatic optimum, LOW – late Oligocene warming, EOT – Eocene–Oligocene transition, EECO – early Eocene climatic optimum, KT – K–T mass extinction, EAIS – east Antarctic ice sheet, AIS – Antarctic ice sheet. The detrended $\delta^{18}\text{O}$ shows the presence of the 13 Myr cycle (red dashed line) between 67 and 17 Ma. (b) Wavelet analysis for detrended $\delta^{18}\text{O}$. White dot line in wavelet power spectrum (left) denotes 13 Myr periodicity and green line is 95% significance contour. Black and red dashed lines in global wavelet spectrum (right) denote 13 Myr periodicity and 95% confidence level. (For interpretation of the references to color in this figure legend, the reader is referred to the web version of this article.)

rate of the sea-floor production (Rowley, 2002), but both processes must be connected because a faster rate of new oceanic crust production should cause an increase in the rate of crust subducted. The production rate wavelet analysis was performed, but is not shown because it does not deliver any statistically significant periods.

Our analysis demonstrates that a periodicity of 13 Myr is common for the geomagnetic reversals, $\delta^{18}\text{O}$ record, and tectonic plate subduction rate. This suggests that there could be a strong connection between the rate of geomagnetic reversals which are indicators of large scale processes in the outer liquid core and subduction rates which are indicators of whole mantle convection coupled to outer core behavior.

Fig. 4 compares the geomagnetic reversal frequency and subduction rate with the detrended $\delta^{18}\text{O}$ record. The geomagnetic reversal frequency (orange dashed line in Fig. 4a) correlates negatively with the $\delta^{18}\text{O}$ record over the Cenozoic Era except during the time interval from 17 Ma to present. The relationship between the subduction rate and the $\delta^{18}\text{O}$ changes is visually unclear in Fig. 4b.

In the past, an arbitrary 0.03 Myr cut-off was used to build the geomagnetic polarity time scale in order to separate geomagnetic polarity reversals from geomagnetic anomalies due to short-term variations (Cande and Kent, 1995). Thus, the GPTS is a smoothed record with filtered out very short geomagnetic events, like geomagnetic excursions and wiggles. It is suggested that the continental ice volume changes may cause geomagnetic excursions by redistributing the Earth's water mass and creating rotational instabilities (Rampino, 1979; Thouveny et al., 2008). The 0.1 Myr cycle

is common in global glacial variations as Milankovitch theory suggests. Some studies demonstrate the presence of the 0.1 Myr eccentricity related cycle in the inclination and intensity of the geomagnetic field changes (Yamazaki and Kanamatsu, 2007; Yamazaki and Oda, 2002; Yokoyama et al., 2010). The geomagnetic events or excursions shorter than 0.1 Myr could be related to the glacial dynamics variations.

The geomagnetic reversal frequency after removing the geomagnetic events shorter than 0.1 Myr (red line in Fig. 4a) is almost equal to the original geomagnetic reversal frequency between 65 Ma and 30 Ma, but becomes lower between 30 Ma and the present. The lower frequency interval coincides with the initiation of the Antarctic ice sheet formation at 34 Ma (Zachos et al., 2001). The differences between the geomagnetic reversal frequency with and without 0.1 Myr rapidly increase to high values 4.5–7 Myr^{-1} after the Miocene climatic optimum (17 to 15 Ma), contrasting with values 2–3 Myr^{-1} during 30–17 Ma. Starting 17 Ma, the global climate undergoes gradual cooling and a major ice sheet in Antarctic establishes by 10 Ma (Zachos et al., 2001). The comparability in the time of Antarctic ice sheet developing and the reversal frequency differences variations further implies that the geomagnetic events shorter than 0.1 Myr may be related to the continental ice sheet dynamics changes. It is, therefore, reasonable to cut off such short-term variations to avoid a conceivable influence by climate changes not solely related to Earth's interior processes.

With further removal of events shorter than 0.1 Myr from the GPTS record we observe much better correspondence between the reversal frequency (red solid line in Fig. 4a) and the detrended $\delta^{18}\text{O}$ records from 65 to present day. Obviously, very short geo-

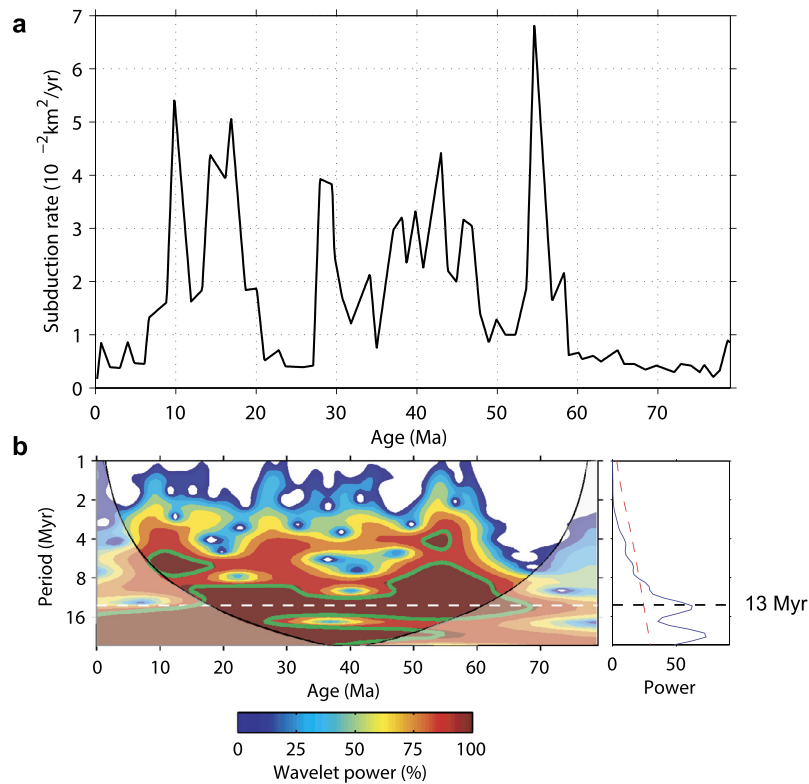


Fig. 3. Variations of subduction rate. (a) Subduction rate of tectonic plates. (b) Wavelet analysis for the subduction rate. White dot line in wavelet power spectrum (left) denotes 13 Myr periodicity and green line is 95% significance contour. Black solid line corresponds to cone of influence, shadowed are outside of the cone. Horizontal white dot line in wavelet power spectrum (left) denotes 13 Myr periodicity. (For interpretation of the references to color in this figure legend, the reader is referred to the web version of this article.)

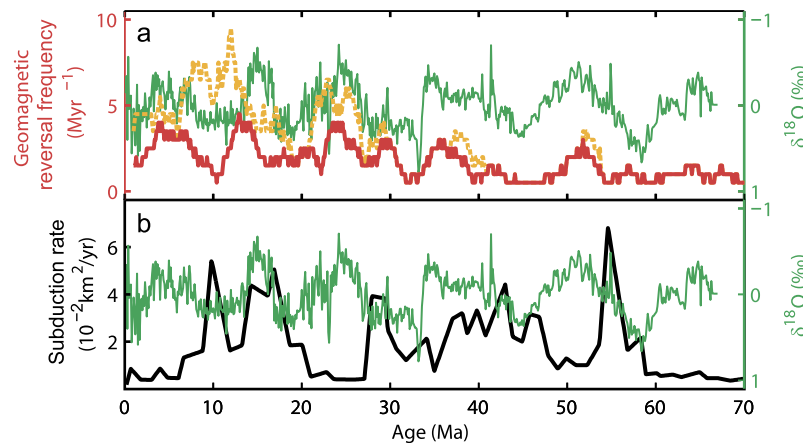


Fig. 4. Comparison of detrended $\delta^{18}\text{O}$, geomagnetic reversal frequency and subduction rate. (a) The geomagnetic reversal frequency with and without the 0.1 Myr cut-off (red and orange lines), and the detrended $\delta^{18}\text{O}$ (green line, note inverted vertical scale). (b) The subduction rate (black line) and the detrended $\delta^{18}\text{O}$ (green line, note inverted vertical scale). (For interpretation of the references to color in this figure legend, the reader is referred to the web version of this article.)

magnetic events (less than 0.1 Myr) recorded with high resolution over the last 17 Myr disturb the correlation between reversal frequency and $\delta^{18}\text{O}$ records which results in a phase difference between 17 Ma and the present that is probably associated with the establishment of the major Antarctic ice sheet after 17 Ma (Zachos et al., 2001; Rampino, 1979; Thouveny et al., 2008).

Wavelet transform coherence is a method for analyzing the coherence and phase lag between two time series as a function of both time and frequency (Grinsted et al., 2004). We use it to estimate the relationships between the detrended $\delta^{18}\text{O}$ record, geomagnetic reversal frequency and subduction rate (Fig. 5). The red band in the periods of 8 to 20 Myr and the leftward arrows in Fig. 5a indicate that the $\delta^{18}\text{O}$ record correlates negatively with

the geomagnetic reversal frequency from 65 to 25 Ma. Fig. 5b is the wavelet coherence between the $\delta^{18}\text{O}$ record and the geomagnetic reversal frequency with the <0.1 Myr event cut-off. The coherent period range in Fig. 5b is still 8–20 Myr, the $\delta^{18}\text{O}$ record and the geomagnetic reversal frequency correlate negatively. Unlike Fig. 5a, the $\delta^{18}\text{O}$ record and the geomagnetic reversal frequency in Fig. 5b correlate well over the Cenozoic Era, and the coherence from 25 Ma to the present improves greatly. The red band in the periods of 8 to 16 Myr and the 55° phase angle at the period of 13 Myr (the upper-rightward arrows) in Fig. 5c suggest that the $\delta^{18}\text{O}$ record correlates positively with the subduction rate with the $\delta^{18}\text{O}$ record leading by ~ 2 Myr at the period of 13 Myr, or the

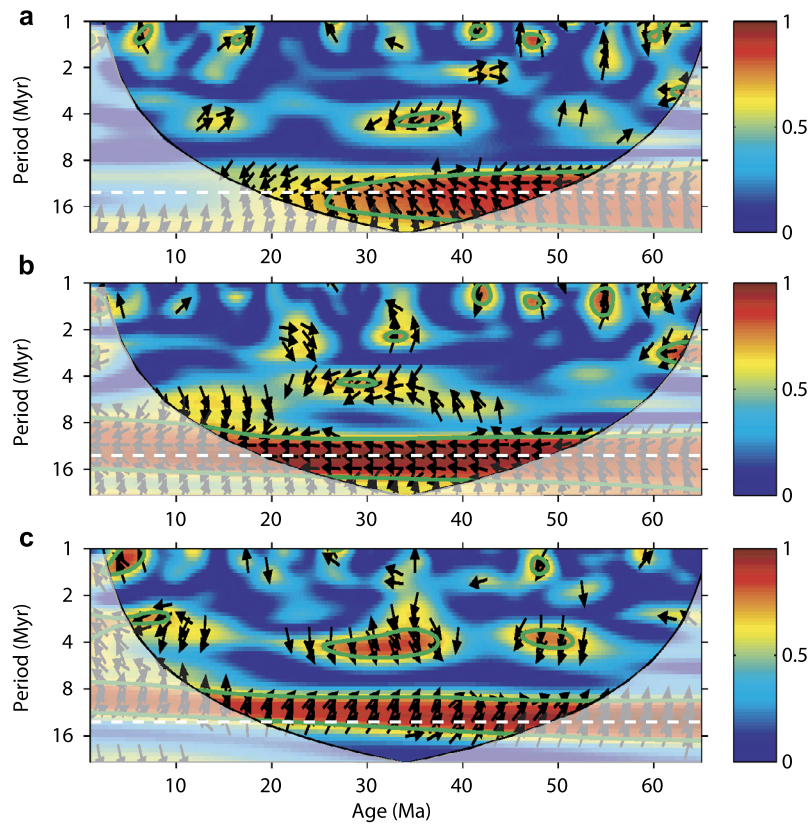


Fig. 5. Wavelet transform coherence using software from Grinsted et al. (2004). (a) Wavelet coherence between the detrended $\delta^{18}\text{O}$ and geomagnetic reversal frequency. (b) Wavelet coherence between the detrended $\delta^{18}\text{O}$ and geomagnetic reversal frequency with <0.1 Myr event cut-off. (c) Wavelet coherence between the detrended $\delta^{18}\text{O}$ and subduction rate. White dashed line denotes the 13 Myr periodicity and the green contour line is the 95% significance contour. Black solid line corresponds to the cone of influence, shadowed area indicates the area outside the cone. A rightward arrow indicates in-phase coherence; a leftward arrow indicates anti-phase coherence; a downward arrow specifies the $\delta^{18}\text{O}$ lagging with the other parameter by 90° and an upward arrow means the $\delta^{18}\text{O}$ leading by 90° . (For interpretation of the references to color in this figure legend, the reader is referred to the web version of this article.)

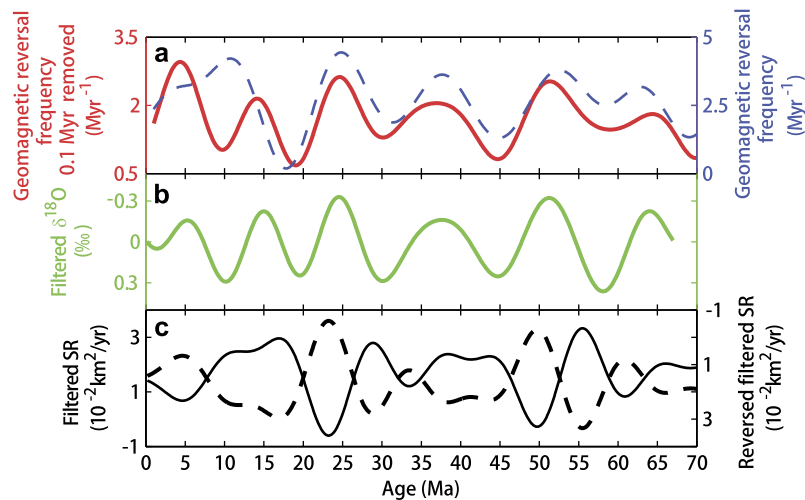


Fig. 6. Comparisons between filtered reversal frequency, $\delta^{18}\text{O}$, and subduction rate of tectonic plates. (a) Filtered reversal frequency (dashed) and filtered reversal frequency after removing intervals shorter than 0.1 Myr. (b) Filtered detrended $\delta^{18}\text{O}$ record. (c) Filtered subduction rate of tectonic plates. All records are filtered using the band-pass filter of 20 and 8 Myr in order to compare the 13 Myr periodicity. (For interpretation of the references to color in this figure legend, the reader is referred to the web version of this article.)

$\delta^{18}\text{O}$ record correlates negatively with the subduction rate with the $\delta^{18}\text{O}$ record lagging by ~ 4.5 Myr.

To compare the relationship between the geomagnetic reversal frequency, detrended $\delta^{18}\text{O}$ variations, and subduction rate on their common periods of 8 to 20 Ma revealed in Fig. 5, we used the bandpass FFT filter, centered at 13 Myr to extract the most prominent period between 20 and 8 Myr. Figs. 6a, b show that the

filtered reversal frequency record (blue dashed line) correlates positively with the filtered detrended $\delta^{18}\text{O}$ record (green line) from 65 to 17 Ma, however, both records show ambiguous phase relationships from 17 Ma to the present. The geomagnetic reversal frequency variations with <0.1 Myr event cut-off (red line) show similar rises and falls over the Cenozoic Era. Fig. 6c shows the variations in the filtered subduction rate (SR). The filtered SR generally

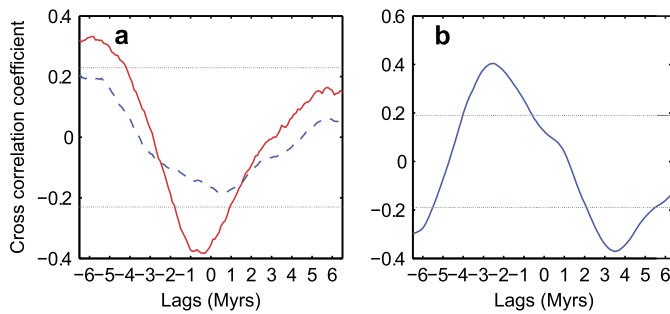


Fig. 7. Cross correlation analysis. (a) Cross correlation between the detrended $\delta^{18}\text{O}$ and geomagnetic reversal frequency records without removal of the geomagnetic events shorter than 0.1 Myr (blue dashed line). Cross correlation between detrended $\delta^{18}\text{O}$ and geomagnetic reversal frequency after removal the chrons shorter than 0.1 Myr (red line). (b) Cross correlation between detrended $\delta^{18}\text{O}$ and subduction rate records. The horizontal dashed lines are the upper and lower confidence bounds, assuming the input series are uncorrelated when compared with 10,000 Monte Carlo simulations of red-noise AR1 data. Correlation coefficients above the confidence bounds are significant ($P < 0.05$). (For interpretation of the references to color in this figure legend, the reader is referred to the web version of this article.)

precedes the reversal frequency and the $\delta^{18}\text{O}$ value, for example, the higher SR at 28 and 55 Ma, respectively correspond to a higher reversal frequency and a lower $\delta^{18}\text{O}$ at 24 and 51 Ma (Fig. 6a, b). However, the inverse of the filtered SR shows a different scenario. The higher reversal frequency and lower $\delta^{18}\text{O}$ variations at 24 and 51 Ma in Fig. 6a, b could alternatively correspond to lower SR at 23 and 49 Ma (Fig. 6c, dashed line).

To estimate the similarities and lags of the geomagnetic reversal frequency and subduction rates with the detrended $\delta^{18}\text{O}$, cross-correlation analysis is used and the result is shown in Fig. 7. The upper and lower confidence bounds are calculated using the Monte-Carlo significance test by comparison made with 10,000 randomly generated red-noise first-order autoregressive data following the method described in Knudsen (2014). The positive correlation coefficient value indicates positive correlation and vice versa. The positive and negative lags mean the reversal frequency or subduction rate variation is ahead of and lags behind of $\delta^{18}\text{O}$ changes, respectively. The blue dashed line in Fig. 7a demonstrates that the reversal frequency without <0.1 Myr event cut-off correlates negatively with the detrended $\delta^{18}\text{O}$ changes, but the correlation coefficient value is lower than the confidence bound (Fig. 7a). The reversal frequency after removing the <0.1 Myr geomagnetic events shown by the red line in Fig. 7a lags behind at ~ 0.5 Myrs and correlates negatively with the detrended $\delta^{18}\text{O}$ changes. However, the 0.5 Myrs lagging is smaller than the 2 Myr slide window when calculating the reversal frequency, and therefore the lagging is not meaningful. The reversal frequency with the <0.1 Myr cut-off could also correlate positively with the $\delta^{18}\text{O}$ record by lagging behind at 5.9 Myrs. The 5.9 Myr lagging is due to both variables with the dominating 13 Myr cycle, and the 5.9 Myrs close to half of a cycle. Fig. 7b shows that subduction rate either correlates negatively with the detrended $\delta^{18}\text{O}$ record, leading by 3.5 Myrs, or correlates positively with the detrended $\delta^{18}\text{O}$ record with 2.5 Myrs lagging behind. Both scenarios are possible and are discussed further in the manuscript.

The estimation of the $\delta^{18}\text{O}$ record lagging and leading the geomagnetic reversal frequency variations at 4.5 and 5 Myr in Fig. 5c is calculated at the period of 13 Myr, while the lagging and leading in the cross correlation in Fig. 7b is the average for all periods, so they slightly differ. The resolutions of both $\delta^{18}\text{O}$ and geomagnetic reversal frequency variations in the cross correlation analysis are 0.1 Myr. In order to compare these parameters with the lower resolution subduction rate data we have to interpolate and resample the million scale resolution of the subduction rate. The estimation

of the $\delta^{18}\text{O}$ record leading and lagging compared to the subduction rate changes cannot be precise nor discussed in detail until better resolution data sets are published in the future.

Fig. 8 summarizes the comparisons between the subduction rates of tectonic plates, detrended $\delta^{18}\text{O}$ record and reversal frequency with the 0.1 Myr event cut-off. The subduction rate is shifted compared to the $\delta^{18}\text{O}$ and geomagnetic reversal frequency variations, as Fig. 7b suggests, and could either correlate negatively or positively with the other two parameters (Fig. 8a). The inversely plotted $\delta^{18}\text{O}$ and reversal frequency variations match well within most of the interval (Fig. 8b).

3. Discussion and conclusions

3.1. Galactic origin of the 13 Myr period

Lewis and Dorne (Lewis, 2006) find that both of the mass extinctions over the last 630 Myrs and beginning of each geologic period are associated with a multiple of the 13 Myr cycle, which they explain in terms of the Oort cloud disturbance when the Sun oscillates vertically through the Galactic disk (Clube and Napier, 1996). It might be one of the explanations of the origin of the 13 Myr cycle. Rampino (2015) suggests that the periodicity of the Sun's vertical oscillations through the Galactic disc is from ~ 30 to 42 Myr. It is still a hypothesis that the 13 Myr cycle and disc dark matter in the Galaxy cause extraterrestrial impacts, mass extinctions and geological events to coincide with each other (Lewis, 2006; Clube and Napier, 1996; Rampino, 2015). Boulila et al. (2012) find a ~ 9 Myr cycle in the Cenozoic $\delta^{13}\text{C}$ record and attribute the cycle to the Earth's long-term orbital eccentricity modulation. We also have a record of 9 Myr cyclicity in the last 23 Ma $\delta^{18}\text{O}$ record. Both the galactic and Earth's orbital change could have impact on Earth's interior and climate change. A possible explanation may arise from the frequency modulation of the Galactic ~ 30 Myr signal with the Earth's ~ 9 Myr long-term eccentricity component ($1/9 - 1/30 = 1/12.9$).

3.2. Connections between subduction, geomagnetic reversals and climate change

The cross-correlation analysis demonstrates that the subduction rate can correlate negatively with the $\delta^{18}\text{O}$ record and with the subduction rate leading by 3.5 Myr, or correlate positively with the $\delta^{18}\text{O}$ record with the subduction rate lagging by 2.5 Myr (Fig. 7). Here we discuss these two possible scenarios.

3.2.1. Subduction rate correlates negatively with the $\delta^{18}\text{O}$ record

Mantle convection is mostly driven by the sinking of cold lithosphere, coupled with a very slow heat counterflow (Parsons and McKenzie, 1978; Richards and Engebretson, 1992). A major portion of the slow counterflow is likely confined to the regions above the Large Low Shear-Velocity Provinces (LLSVPs) (Trønnes, 2010). The heat flux at the bottom boundary is shown to be strongly correlated with the advection due to cold plumes (Labrosse, 2002). Sinking slabs eventually arrive at the low mantle, displacing material and thinning the thermal boundary layer at the base of the mantle (Goes et al., 2008). This increases the thermal conductivity of the lowermost mantle and increases the CMB heat flux (Biggin et al., 2012; Steinberger and Torsvik, 2012). An increase in CMB heat flux might be caused by enhanced subduction, and a relatively low CMB heat flux might result from reduced subduction (Zhang and Zhong, 2011). Geodynamo simulations suggest that transitions from periods of rapid polarity reversals to periods of prolonged stability are triggered by decreases in CMB heat flow (Courtilot and Olson, 2007; Biggin et al., 2012; Wicht and Olson, 2004), i.e. lower CMB heat flow corresponds to

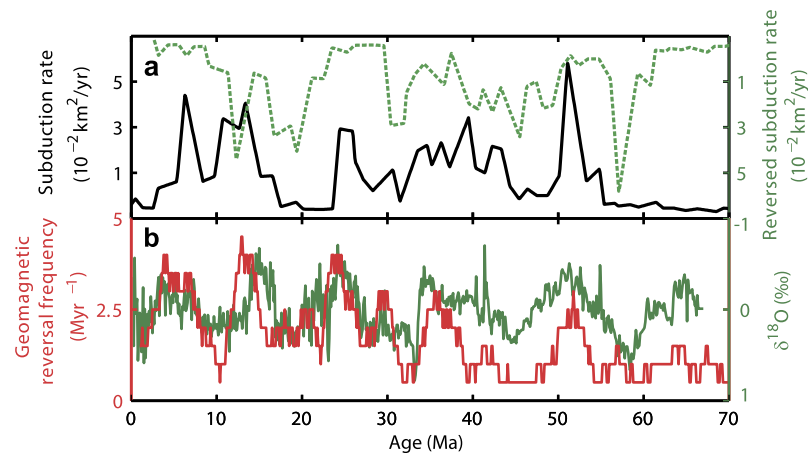


Fig. 8. Comparison between the subduction rate of tectonic plates, detrended $\delta^{18}\text{O}$, and geomagnetic reversal frequency. (a) Subduction rate of tectonic plates the age of SR offset is -3.5 Myrs (line) and 2.5 Myrs (dashed line); (b) reversal frequency after removing events shorter than 0.1 Myr (red line) and detrended $\delta^{18}\text{O}$ (green line). (For interpretation of the references to color in this figure legend, the reader is referred to the web version of this article.)

the lower reversal frequency and vice versa. The higher subduction rate may lead to the higher CMB heat flux and higher reversal frequency.

Hot plumes are formed at the core–mantle boundary due to sinking of the cold lithosphere that allows the concentration of hot matter. The proportion of heat transported by hot plumes is estimated at $10\text{--}15\%$ relative to total upwards heat flow (Davies, 1998). An order of magnitude higher heat flux in the large number of seamount volcanoes, additional to the heat transport in the LLSVPs, was also suggested (Malamud and Turcotte, 1999). The large number of seamount volcanoes release CO_2 , SO_2 , and thermogenic gases and facilitate the warming of the Earth. The quantity of CO_2 present in the atmosphere has been proposed to be the reason for the Cenozoic climatic transitions, e.g., EOT, EECO (Zachos et al., 2008; DeConto and Pollard, 2003). Higher subduction rate results in the higher reversal frequency and warmer climate (i.e. lower $\delta^{18}\text{O}$). Hence, subduction rate should be ahead of $\delta^{18}\text{O}$ and correlates negatively with it. The heat flow and volcanic activity combined appear to be a possible cause of the similar rhythms of reversal frequency, climate change and subduction rate on million years scale.

Modeling results indicate that the sinking slabs, after the subduction initiation, take approximately $30\text{--}50$ Myr to reach the low mantle (Biggin et al., 2012; Zhang and Zhong, 2011). Plume rise time from CMB to the surface varies between 5 and 100 Myrs (Olson et al., 1987; Thompson and Tackley, 1998) or 20 and 50 Myrs (Van Hinsbergen et al., 2011). Here the high reversals frequency and warm climate changes are in phase, and the subduction rate increase leads ahead of both parameters by 3.5 Myr. The 3.5 Myr subduction rate leading other parameters is too short of a time interval to allow the sinking slab to reach the core mantle boundary and/or the hot plume to rise to the surface. This plume-link explanation seems unrealistic in the context of our present understanding of the deep mantle plume processes.

3.2.2. Subduction rate correlated positively with the $\delta^{18}\text{O}$

The long-term cycle makes the Earth's core capture the disc dark matter in the Galaxy and become hotter periodically. The Episodic heating of the Earth's core alters the status of the geodynamo and thus triggers the frequency of geomagnetic reversals (Rampino, 2015). The geomagnetic field is significantly weaken, dropping its strength, when the geomagnetic reversals occur (Nowaczyk et al., 2012). When the geomagnetic field intensity is lower, the planetary ionosphere directly interacts with solar wind and ions escape (Wei et al., 2012). For example, high-frequency geomagnetic reversals continually enhance oxygen es-

cape rate by $3\text{--}4$ orders higher than today, and this cumulative effect could cause a significant drop of oxygen level (Wei et al., 2014). The shortwave scattering by air molecules and clouds is less frequent under the lower partial pressure of oxygen and the reduced-density atmosphere. The surface shortwave forcing increases significantly, and results in high atmospheric water vapor and enhances greenhouse forcing the global surface temperature to rise (Poulsen et al., 2015). Thus, the higher geomagnetic reversal frequency is able to rise global temperature by reducing the geomagnetic field intensity and increasing the solar wind effects. It explains why the variations of the geomagnetic reversal frequency and temperature are almost synchronous in this model.

Crowley et al. (2015) find the production of the oceanic crust at mid-ocean ridges response to periodic ice ages and sea level changes which are regulated by the well-known Milankovitch cycles related to the Earth's orbital changes. Their model suggests that higher sea level increases the overlying pressure of sea floor, and suppresses the eruption of magma. It indicates that warmer climate (lower $\delta^{18}\text{O}$) and corresponding higher sea level could result in the lower crust production and subduction rate. Hence, the subduction rate could correlate positively with $\delta^{18}\text{O}$ and lag behind the climate changes.

4. Conclusions

We propose that geomagnetic reversals (as indicators of CMB heat flux increase), climate change, and subduction rates are closely associated with each other on a ten million years scale. The cycles for geomagnetic reversal frequency and long-term climate changes occur with similar rise and fall with a fundamental periodicity of ~ 13 Myr in the Cenozoic Era. The subduction rate has the same periodicity but slightly leads or lags behind; we provide tentative explanations for both scenarios. In the first scenario, higher subduction rate produces higher CMB heat flux and reversal frequency due to the subduction slab sinking. It also leads to stronger mantle plume activity and consequently warmer climate and lower $\delta^{18}\text{O}$. The time of the subduction slab sinking and plume rising are far longer than that of the subduction leading $\delta^{18}\text{O}$, so this scenario seems improbable at the level of our present day knowledge about the mantle dynamics. In the second scenario, the 13 Myr cycle could be due to the variations of solar system's galactic orbit. Passage of the Earth through dark matter in the Galactic plane could lead to heating in the core and consequently a higher reversal rate. The higher frequency of geomagnetic reversals and lower geomagnetic field intensity may lead to ions escaping from the atmosphere and higher shortwave forcing with

higher atmospheric water vapor. Such process would lead to the warmer climate (lower $\delta^{18}\text{O}$), higher sea level and consequently higher overlying pressure which transfers to lower rate of magma eruption and lower subduction rate.

Acknowledgements

We thank the National Science Foundation of China grants of X.L. (NSFC grants 41210002, U1405231, 40830105, 41202129), the Natural Sciences and Engineering Research Council of Canada of V.A.K. (NSERC RGPIN-2014-04183) and the University of Alberta for support of this study. The China Scholarship Council supported the joint China/Canada Ph.D. program for J.C. (grant 2011618125).

References

- Berner, R.A., Lasaga, A.C., Garrels, R.M., 1983. The carbonate–silicate geochemical cycle and its effect on atmospheric carbon dioxide over the past 100 million years. *Am. J. Sci.* 283, 641–683.
- Biggin, A., Steinberger, B., Aubert, J., Suttie, N., Holme, R., Torsvik, T., van der Meer, D., van Hinsbergen, D., 2012. Possible links between long-term geomagnetic variations and whole-mantle convection processes. *Nat. Geosci.* 5, 526–533.
- Boullie, S., Galbrun, B., Laskar, J., Pälike, H., 2012. A ~9 myr cycle in Cenozoic $\delta^{13}\text{C}$ record and long-term orbital eccentricity modulation: is there a link? *Earth Planet. Sci. Lett.* 317 (318), 273–281.
- Cande, S.C., Kent, D.V., 1995. Revised calibration of the geomagnetic polarity timescale for the Late Cretaceous and Cenozoic. *J. Geophys. Res., Solid Earth* 100, 6093–6095.
- Clube, S., Napier, W., 1996. Galactic dark matter and terrestrial periodicities. *Q. J. R. Astron. Soc.* 37, 617.
- Courtilot, V., Olson, P., 2007. Mantle plumes link magnetic superchrons to Phanerozoic mass depletion events. *Earth Planet. Sci. Lett.* 260, 495–504.
- Crowley, J.W., Katz, R.F., Huybers, P., Langmuir, C.H., Park, S.-H., 2015. Glacial cycles drive variations in the production of oceanic crust. *Science* 347, 1237–1240.
- Davies, G.F., 1998. Plates, plumes, mantle convection and mantle evolution. In: *The Earth's Mantle: Composition, Structure and Evolution*, pp. 228–229.
- DeConto, R.M., Pollard, D., 2003. Rapid Cenozoic glaciation of Antarctica induced by declining atmospheric CO_2 . *Nature* 421, 245–249.
- Gaffin, S., 1987. Phase difference between sea level and magnetic reversal rate. *Nature* 329, 816–819.
- Garzione, C.N., 2008. Surface uplift of Tibet and Cenozoic global cooling. *Geology* 36, 1003–1004.
- Gee, J.S., Kent, D.V., 2007. Source of oceanic magnetic anomalies and the geomagnetic polarity time scale. *Treatise on Geophysics*, vol. 5: Geomagnetism, 455–507.
- Goes, S., Capitanio, F.A., Morra, G., 2008. Evidence of lower-mantle slab penetration phases in plate motions. *Nature* 451, 981–984.
- Grinsted, A., Moore, J.C., Jevrejeva, S., 2004. Application of the cross wavelet transform and wavelet coherence to geophysical time series. *Nonlinear Process. Geophys.* 11, 561–566.
- Knudsen, M.F., 2014. Evidence for external forcing of the Atlantic multidecadal oscillation since termination of the Little Ice Age. *Nat. Commun.* 5, 163–180.
- Labrosse, S., 2002. Hotspots, mantle plumes and core heat loss. *Earth Planet. Sci. Lett.* 199, 147–156.
- Lewis, D.F., 2006. The astronomical pulse of global extinction events. *Sci. World J.* 6, 718–726.
- Malamud, B.D., Turcotte, D.L., 1999. How many plumes are there? *Earth Planet. Sci. Lett.* 174, 113–124.
- Marzocchi, W., Mulargia, F., 1992. The periodicity of geomagnetic reversals. *Phys. Earth Planet. Inter.* 73, 222–228.
- Mazaud, A., Laj, C., 1991. The 15 m.y. geomagnetic reversal periodicity: a quantitative test. *Earth Planet. Sci. Lett.* 107, 689–696.
- Mazaud, A., Laj, C., de Seze, L., Verosub, K.L., 1983. 15-Myr periodicity in the frequency of geomagnetic reversals since 100 Myr. *Nature* 304, 328–330.
- Nowaczyk, N.R., Arz, H.W., Frank, U., Kind, J., Plessen, B., 2012. Dynamics of the Laschamp geomagnetic excursion from Black Sea sediments. *Earth Planet. Sci. Lett.* 351 (352), 54–69.
- Olson, P., Schubert, G., Anderson, C., 1987. Plume formation in the D-layer and the roughness of the core mantle boundary. *Nature*, 409–413.
- Pal, P.C., Creer, K.M., 1986. Geomagnetic reversal spurts and episodes of extraterrestrial catastrophism. *Nature* 320, 148–150.
- Parsons, B., McKenzie, D., 1978. Mantle convection and the thermal structure of the plates. *J. Geophys. Res., Solid Earth* 83, 4485–4496.
- Poulsen, C.J., Tabor, C., White, J.D., 2015. Long-term climate forcing by atmospheric oxygen concentrations. *Science* 348, 1238–1241.
- Rampino, M.R., 1979. Possible relationships between changes in global ice volume, geomagnetic excursions, and the eccentricity of the Earth's orbit. *Geology* 7, 584–587.
- Rampino, M.R., 2015. Disc dark matter in the Galaxy and potential cycles of extraterrestrial impacts, mass extinctions and geological events. *Mon. Not. R. Astron. Soc.* 448, 1816–1820.
- Rampino, M.R., Prokoph, A., 2013. Are mantle plumes periodic? *Eos* 94, 113–114.
- Rampino, M.R., Stothers, R.B., 1987. Episodic nature of the Cenozoic marine record. *Paleoceanography* 2, 255–258.
- Rampino, M.R., Stothers, R.B., 1984. Geological rhythms and cometary impacts. *Science* 226, 1427–1431.
- Richards, M.A., Engebretson, D.C., 1992. Large-scale mantle convection and the history of subduction. *Nature* 355, 437–440.
- Rowley, D.B., 2002. Rate of plate creation and destruction: 180 Ma to present. *Geol. Soc. Am. Bull.* 114, 927–933.
- Sobolev, S.V., Sobolev, A.V., Kuzmin, D.V., Krivolutskaya, N.A., Petrunin, A.G., Arndt, N.T., Radko, V.A., Vasiliev, Y.R., 2011. Linking mantle plumes, large igneous provinces and environmental catastrophes. *Nature* 477, 312–316.
- Steinberger, B., Torsvik, T.H., 2012. A geodynamic model of plumes from the margins of Large Low Shear Velocity Provinces. *Geochem. Geophys. Geosyst.* 13, Q01W09.
- Thompson, P.F., Tackley, P.J., 1998. Generation of mega-plumes from the core–mantle boundary in a compressible mantle with temperature-dependent viscosity. *Geophys. Res. Lett.* 25, 1999–2002.
- Thouveny, N., Bourlès, D.L., Saracco, G., Carcaillet, J.T., Bassinot, F., 2008. Paleoclimatic context of geomagnetic dipole lows and excursions in the Brunhes, clue for an orbital influence on the geodynamo? *Earth Planet. Sci. Lett.* 275, 269–284.
- Torrence, C., Compo, G.P., 1998. A practical guide to wavelet analysis. *Bull. Am. Meteorol. Soc.* 79, 61–78.
- Trønnes, R., 2010. Structure, mineralogy and dynamics of the lowermost mantle. *Mineral. Petrol.* 99, 243–261.
- Van Hinsbergen, D.J.J., Steinberger, B., Doubrovine, P.V., Gassmüller, R., 2011. Acceleration and deceleration of India–Asia convergence since the Cretaceous: roles of mantle plumes and continental collision. *J. Geophys. Res., Atmos.* 116, 100–114.
- Vine, F.J., Matthews, D.H., 1963. Magnetic anomalies over oceanic ridges. *Nature* 199, 947–949.
- Wei, Y., Fraenz, M., Dubinin, E., Woch, J., Lühr, H., Wan, W., Zong, Q.G., Zhang, T.L., Pu, Z.Y., Fu, S.Y., 2012. Enhanced atmospheric oxygen outflow on Earth and Mars driven by a corotating interaction region. *J. Geophys. Res. Space Phys.* 117.
- Wei, Y., Pu, Z., Zong, Q., Wan, W., Ren, Z., Fraenz, M., Dubinin, E., Tian, F., Shi, Q., Fu, S., Hong, M., 2014. Oxygen escape from the Earth during geomagnetic reversals: implications for mass extinction. *Earth Planet. Sci. Lett.* 394, 94–98.
- Wicht, J., Olson, P., 2004. A detailed study of the polarity reversal mechanism in a numerical dynamo model. *Geochem. Geophys. Geosyst.* 5, 223–229.
- Yamazaki, T., Kanamatsu, T., 2007. A relative paleointensity record of the geomagnetic field since 1.6 Ma from the North Pacific. *Earth Planets Space* 59, 785–794.
- Yamazaki, T., Oda, H., 2002. Orbital influence on Earth's magnetic field: 100,000-year periodicity in inclination. *Science* 295, 2435–2438.
- Yokoyama, Y., Yamazaki, T., Oda, H., 2010. Geomagnetic 100-kyr variation excited by a change in the Earth's orbital eccentricity. *Geophys. Res. Lett.* 37.
- Zachos, J., Pagani, M., Sloan, L., Thomas, E., Billups, K., 2001. Trends, rhythms, and aberrations in global climate 65 Ma to present. *Science* 292, 686–693.
- Zachos, J.C., Dickens, G.R., Zeebe, R.E., 2008. An early Cenozoic perspective on greenhouse warming and carbon-cycle dynamics. *Nature* 451, 279–283.
- Zhang, N., Zhong, S., 2011. Heat fluxes at the Earth's surface and core–mantle boundary since Pangea formation and their implications for the geomagnetic superchrons. *Earth Planet. Sci. Lett.* 306, 205–216.